ELSEVIER

Journal of Power Sources 83 (1999) 114–120

JOURNAL OF POWER SOURCES

www.elsevier.com/locate/jpowsour

Cycle life and utilization studies on cobalt microencapsulated AB_5 type metal hydride

Anand Durairajan, Bala S. Haran, Branko N. Popov *, Ralph E. White

Department of Chemical Engineering, University of South Carolina, Columbia, SC 29208, USA

Received 15 January 1999; received in revised form 31 March 1999; accepted 31 March 1999

Abstract

$LaNi_{4.27}Sn_{0.24}$ alloy was microencapsulated with cobalt by electroless deposition. The coated material has a higher capacity compared to the bare alloy due to the faradaic reaction of cobalt during discharge. This additional capacity has been studied using various material and electrochemical characterization techniques. The capacity due to cobalt varies depending on the amount of active material available for reaction. An increase in utilization is seen with decrease in thickness of the coating. Active surface area and the transport process within the film control the amount of cobalt utilized. Finally, cobalt coated alloys are seen to cycle ten times more than bare $LaNi_{4.24}Sn_{0.27}$ with constant capacity.

Keywords: Cobalt; Metal hydride; $LaNi_{4.27}Sn_{0.24}$

1. Introduction

Nickel–hydrogen batteries with a hydrogen storing alloy as negative electrode was first proposed by Justi et al. in 1970 [1]. Environmental concerns and low energy density of Ni–Cd batteries has speeded up research in metal hydride alloys. Metal hydrides also possess other advantages like tolerance to overcharge and over discharge, high rate capability, etc. [2]. The typical AB_5 type hydrogen storage alloy is a transition metal nickel alloyed with a rare earth metal like lanthanum or several rare earth metals. However, the hydrogen storage capacity of this alloy declines drastically during cycling.

Alloy pulverization and oxidation have been reported as the important causes for capacity decay [3]. Alloy pulverization is the breaking of metal hydride alloy particles during cycling. This is believed to be because of the continuous lattice expansion/contraction during cycling. Many investigators have shown that the cycling stability of $LaNi_5$ could be improved by partial substitution of nickel by silicon, aluminium, manganese, cobalt and other elements [3–5]. These substitutions reduce the volume expansion during cycling and hence increase the stability. However, substitutions lower the reversible capacity leading to a decrease in energy density. They also do not provide the necessary corrosion resistance to the alloy. Cycle life studies on $LaNi_{4.27}Sn_{0.24}$ done by Durairajan et al. [6] show the loss of 50% of capacity in less than 50 cycles. Cobalt substitution has been shown to be most beneficial to the performance of the metal hydride as a battery electrode [7,8]. Apart from reducing the volume expansion, previous investigators have found the formation of $Co(OH)_2$ during cycling which had beneficial effects on the alloy cycle life [9].

While numerous studies exist on different amounts of cobalt and other metal substitutions, very few focus on the role of cobalt coatings. Microencapsulation or surface coating of metal hydride alloys with various metals (Cu, Ni, Pd, Co) has shown to be effective for improving electrode properties such as discharge capacity, cycle life and rate capability [7,10–12]. However, coating with Ni, Cu, Pd increases the dead weight of the electrode and reduces the net energy density. On the other hand, cobalt encapsulation leads to superior alloys with increased capacity and cycle life [7].

Studies on electroless cobalt coatings for microencapsulation of metal hydrides by Haran et al. [7] have shown the beneficial effects of cobalt on cycle life of AB_5 alloys. However, the role of cobalt on alloy protection and on improving the cycle life has not been studied.

* Corresponding author. Tel.: +1-803-777-7314; fax: +1-803-777-8265; E-mail: popov@engr.sc.edu

0378-7753/99/$ - see front matter
PII: S0378-7753(99)00283-9

In this work, we encapsulate $LaNi_{4.27}Sn_{0.24}$ alloy with cobalt and investigate the cobalt faradaic reaction and the capacity achieved by it. Utilization studies were done with an aim to maximize the capacity of the cobalt coatings. Electron Probe MicroAnalysis (EPMA) has been used to explain the effects of cobalt on cycle life of the alloy.

2. Experimental

$LaNi_{4.27}Sn_{0.24}$ alloy particles were ground and sieved to obtain particles of size 90–106 μm. Cobalt encapsulation was carried out with moderate stirring in 20 g/l cobalt sulfate, 20 g/l sodium hypophosphite, 50 g/l sodium citrate and 40 g/l ammonium chloride. In addition to these constituents, NH_4OH was added periodically during deposition to maintain the pH between 8.5 and 9.5. The pH frequently dropped below 9 during deposition indicating that cobalt deposition was proceeding. The deposition was stopped once the pH remained constant, indicating the absence of cobalt in the solution. The alloy powder was rinsed with deionized water, filtered and dried at 65°C. EPMA was used to characterize the thickness of the deposits obtained. Particle size was measured using Laser Particle Size Analyzer. Pellet electrodes were obtained by hot pressing the encapsulated and bare $LaNi_{4.27}Sn_{0.24}$ alloy between two-nickel meshes with 5% PTFE binder. The compacting pressure (6 tonnes/cm^2) and heating insured the homogeneity and mechanical integrity of the pellet electrode. Electrochemical characterization studies were done in a three-electrode set up with NiOOH counter electrode and Hg/HgO reference electrode. All potentials unless specified are referred to the Hg/HgO reference electrode. A 6 M KOH was used as the electrolyte. Hydrogen storage capabilities of cobalt coated and bare $LaNi_{4.27}Sn_{0.24}$ alloy were monitored by measuring the charge/discharge characteristics of the electrode. Cycle life studies were done using a Bitrode LCN battery-testing module under a constant temperature of 25°C. The working electrodes were activated for hydride formation by continuous galvanostatic cycling until a constant value of the hydrogen storage capacity was obtained. The discharge cut-off potential was maintained at −0.6 V for all electrochemical tests. Charge–discharge studies were done at a 0.1 C rate, while the cycle life studies were carried out at a 0.3 C rate.

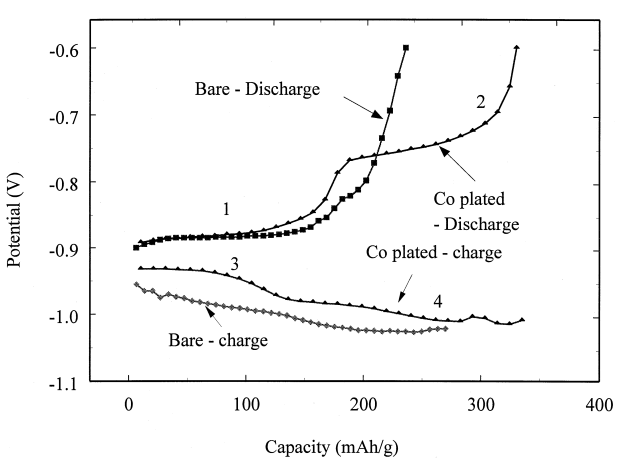

Fig. 1. Charge–discharge characteristics of cobalt coated and bare $LaNi_{4.27}Sn_{0.24}$ alloy electrodes. The increased capacity in case of cobalt plated alloy is due to the $Co/Co(OH)_2$ faradaic reaction.

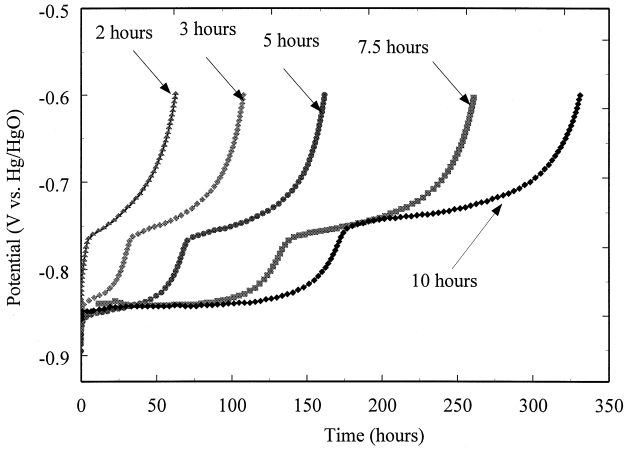

Fig. 2. Discharge studies on cobalt coated $LaNi_{4.27}Sn_{0.24}$ alloy electrode for different charging times.

3. Results and discussion

3.1. Charge–discharge characteristics

The hydrogen absorption/desorption reaction is given by:

$$MH_{x,ads} + xOH^- \underset{\text{charge}}{\overset{\text{discharge}}{\leftrightarrow}} M + xH_2O + xe^- \qquad E = -930\,\text{mV vs. Hg/HgO} \quad (1)$$

The behavior of cobalt metal in alkaline solutions has been studied in detail. Popov et al. [13,14] have shown that the anodic oxidation of cobalt in aqueous solutions results in a variety of oxides. The type of oxide depends on the potential of oxidation. Cyclic voltammograms on pure cobalt by Simpraga [15] reveals three major anodic peaks. As the potential is swept from −0.2 V to +1.6 V vs. reversible hydrogen electrode (RHE), various species are formed namely — $Co(OH)_2$ (−0.3 V), Co(OOH), Co_3O_4 (1.05 V). Cobalt undergoes different valency changes as the oxidation potential is varied.

In our case, the reaction of interest occurs during the initial stages of oxidation at −0.8 V vs. Hg/HgO. This is

Table 1
Charge–discharge studies on cobalt coated $LaNi_{4.27}Sn_{0.24}$ at a 0.1 C rate

Charge time (h)	Total discharge capacity (mA h/g)	Discharge capacity due to hydride (mA h/g)	Discharge capacity due to cobalt (mA h/g)
10	336	175.05	160.95
7.5	261.00	135.59	125.41
5	161.92	69.20	92.72
3	107.63	30.54	77.09
2	62.56	7.91	54.65

the conversion of cobalt to cobalt hydroxide in a two-electron process.

$$Co + 2OH^- \underset{Rdn}{\overset{Oxdn}{\leftrightarrow}} Co(OH)_2 + 2e^- \quad (2)$$

At these potentials, $Co(OH)_2$, owing to its low standard free enthalpy of formation ($-109\,000$ cal.@25°C), is the most stable form of oxide [16]. The potential window of operation during discharge of a MH electrode is -0.9 to -0.6 V. Cobalt oxidation to $Co(OH)_2$ occurs within this voltage range.

The two reactions due to metal hydride (Eq. (1)) and cobalt (Eq. (2)) are shown as two potential plateaus (1 and 2) in the discharge curve shown in Fig. 1. The discharge curve for bare alloy is also given for comparison. The metal hydride discharge reaction proceeds first because of the more negative equilibrium potential (reaction 1, Fig. 1). The cobalt oxidation reaction 2, shown in Fig. 1, starts only after the hydrogen concentration in the metal hydride becomes negligible. The cobalt oxidation reaction begins at a potential of -800 mV vs. Hg/HgO and proceeds till all available cobalt is utilized. Diffusion limitations set in at the end of both of these discharge reactions. The discharge curves were highly repetitive indicating the reversibility of this faradaic reaction. The charge curve shows the reduction of $Co(OH)_2$ to cobalt. Haran et al. [7] observed the complete conversion of $Co(OH)_2$ to Co during successive charge cycles. During charging, the reverse of discharge happens namely all the $Co(OH)_2$ is first reduced to Co and subsequently hydriding of $LaNi_{4.24}Sn_{0.27}$ alloy begins. This is in agreement with the thermodynamic potentials of Eqs. (1) and (2).

Fig. 2 shows the discharge profiles of cobalt coated $LaNi_{4.27}Sn_{0.24}$ for various charging times. For lower times of charging, only the cobalt faradaic reaction is seen during discharge. This is due to the fact that $Co(OH)_2/Co$ reaction occurs at a lower potential than the hydrogen evolution reaction. As charging time is increased gradually, all the available cobalt hydroxide is brought back to cobalt and the potential proceeds to hydrogen evolution. The increase in metal hydride utilization and capacity due to cobalt for different charging times are shown in Table 1.

The theoretical capacity that can be achieved by the cobalt oxidation reaction can be calculated simply by Faraday's law. Based on a two-electron reaction, this is seen to be 900 mA h/g. However, the capacity that is realized from cobalt during the discharge of cobalt coated electrode is much less (480 mA h/g). The reduced utilization of cobalt arises due to various limitations, some of which are discussed later.

Weizhong et al. [8] have reported an increase in electrochemical capacity of the hydride electrode due to mixing with cobalt. In order to study the effect of cobalt mixing on the performance of metal hydride alloys, 25 wt.% cobalt was mixed with $LaNi_{4.27}Sn_{0.24}$ alloy. Fig. 3 shows

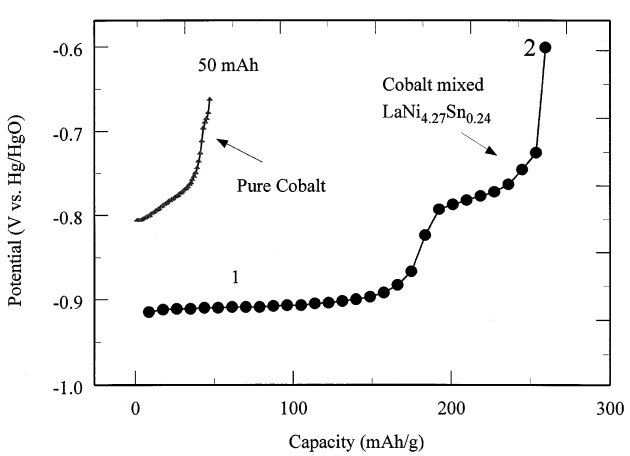

Fig. 3. Discharge profile of cobalt mixed $LaNi_{4.27}Sn_{0.24}$ alloy. Discharge curve of pure cobalt electrode is also shown for comparison.

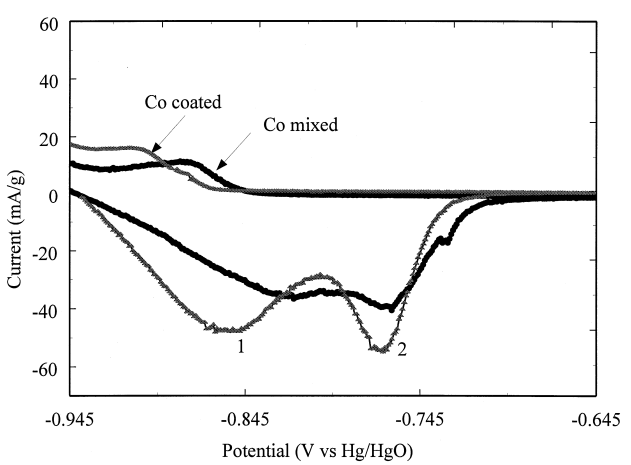

Fig. 4. Cyclic voltammograms of cobalt encapsulated and cobalt mixed $LaNi_{4.27}Sn_{0.24}$ electrode before activation.

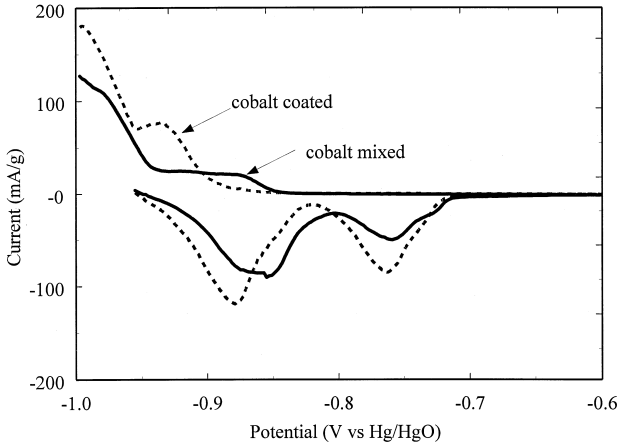

Fig. 5. Cyclic voltammograms of fully activated cobalt encapsulated and cobalt mixed $LaNi_{4.27}Sn_{0.24}$ electrode before activation. The second peak is due to $Co/Co(OH)_2$ reaction.

the discharge profile of cobalt mixed $LaNi_{4.27}Sn_{0.24}$ alloy electrode. The second plateau due to the cobalt reaction appears at the equilibrium potential for cobalt oxidation reaction. However, capacity due to cobalt is much lesser in this case than that of encapsulation. A comparison of Figs. 1 and 3 clearly shows the presence of same type of reactions with equal MH discharge plateaus and larger cobalt discharge plateau in case of encapsulation. Discharge curve of pure cobalt (<2 μm size) cycled under the similar conditions is shown for comparison. This discharge curve is exactly similar to the second plateau observed during the discharge of cobalt plated and cobalt mixed electrodes in Figs. 1 and 3, respectively. These studies clearly show that the second plateau is purely due to the cobalt faradaic reaction. The capacity of the cobalt mixed $LaNi_{4.27}Sn_{0.24}$ alloy electrode is calculated to be 260 mA h/g. The capacity that is realized due to pure cobalt in Fig. 2a is very small (50 mA h/g).

Although mixing cobalt with metal hydride alloy leads to an additional capacity, this does not provide the corrosion protection of cobalt microencapsulation. This is discussed further in cycle life studies.

3.2. Cyclic voltammograms

Cyclic voltammograms on the pellet electrode were obtained at a low scan rate of 0.01 mV/s. Pellet electrodes were initially charged at 0.1 C rate to their full capacity. This ensures the reduction of all cobalt oxides to the elemental form [7]. The potential was swept from −1.0 V to −0.6 V and back to −1.0 V. The potential range of −0.6 to −1.0 V represents the stable region for the $LaNi_{4.27}Sn_{0.24}$ alloy where the alloy is not oxidized. Fig. 4 shows the CV of cobalt microencapsulated and 25% cobalt (<2 μm) mixed $LaNi_{4.27}Sn_{0.24}$ electrode before activation. The CV is characterized by the presence of two peaks in the forward and reverse scans. The first peak on sweeping the potential to more positive values corresponds to hydrogen desorption from the electrode. The very low scan rate allows sufficient time for hydrogen diffusion from the bulk to the surface of the alloy. Cobalt oxidation reaction proceeds thereafter and a peak current is observed at around −0.76 V. The reverse sweep (−0.6 V to −1.1 V) is characterized by the presence of $Co(OH)_2$ reduction and hydrogen absorption reactions. The reduction of $Co(OH)_2$ to Co starts at around −0.89 V and proceeds till all $Co(OH)_2$ is brought back to cobalt. After this reduction reaction, hydrogen evolution starts. This shows the reversibility of the reaction, which is also seen from the repetitive discharge curves.

Fig. 5 shows the CVs of cobalt coated and cobalt mixed $LaNi_{4.27}Sn_{0.24}$ electrode after conditioning. The CVs were done under exactly similar conditions as before. The forward sweep as well as the reverse sweep shows the presence of two reactions on the electrode surface. However, the peak currents representing the electrode reactions are large compared to the previous case. This is due to the improved kinetics and storage capacity after activation [17].

The cobalt reaction peak in the mixed electrode is small compared to the encapsulated electrode. This is due to the following reasons. The diffusion of hydroxyl ions through the cobalt during the cobalt oxidation reactions is greatly determined by the particle size or the thickness of cobalt. Also the surface area per unit weight of cobalt influences the cobalt utilization. These factors are discussed in a more detailed manner using the next set of studies.

3.3. Cobalt utilization studies

The discharge behavior of pure cobalt (Fig. 3) resembles the second discharge plateau of cobalt plated $LaNi_{4.27}Sn_{0.24}$ electrode (Fig. 1). However, the utilization of cobalt in the former case is much lesser than that

Table 2
Effect of coating thickness on the capacity utilization of cobalt

Coating thickness (μm)	Capacity due to cobalt (mA h/g)	Cobalt utilization (%)[a]	Cycle life
0.285	710	78.89	40
0.338	640	71.11	60
0.345	600	66.67	90
0.789	580	64.44	200 +

[a] Cobalt utilization = [(Capacity due to cobalt)/(Theoretical Co capacity (900 mA h/g))] × 100%.

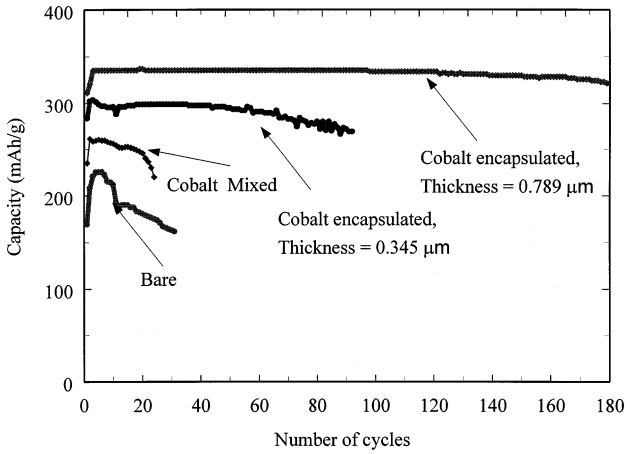

Fig. 6. Cycle life studies on cobalt encapsulated and bare $LaNi_{4.27}Sn_{0.24}$ alloy electrodes. The electrodes were cycled at 0.3 C rate in 6 M KOH electrolyte.

obtained with cobalt encapsulation. Pure cobalt used for this study was crystalline in nature and was of size 2 μm. It is well known that electroless deposition leads to amorphous deposits due to codeposition of two or more elements. In general an amorphous structure aids in faster transport of active species as compared to crystalline material. This partly aids in better utilization of cobalt deposits as compared to pure cobalt. Thicknesses of cobalt films obtained as a result of microencapsulation are very much below 1 μm (Table 2). The large surface area available for reaction contributes significantly for the enhanced utilization of the thin cobalt films. The deposition thickness was varied initially by varying the composition of cobalt. More amount of cobalt on the same surface area of $LaNi_{4.27}Sn_{0.24}$ alloy gives thicker coatings. EPMA was adopted to estimate the thickness of cobalt coatings in microencapsulated alloys. Table 2 presents the cobalt capacity utilization for various thicknesses of films. It is seen that very thin films of cobalt can give large capacity utilizations. This is due to the fact that a small amount of cobalt is spread over a large surface area. Hence, more amount of cobalt is exposed to the electrolyte. However, for thicker coatings more amount of cobalt is deposited over the same surface area. This leads to lesser reaction of cobalt with the electrolyte and hence lower utilization.

3.4. Cycle life studies

The pellets were cycled at 0.3 C charge–discharge rate after the activation and preliminary characterization stud-

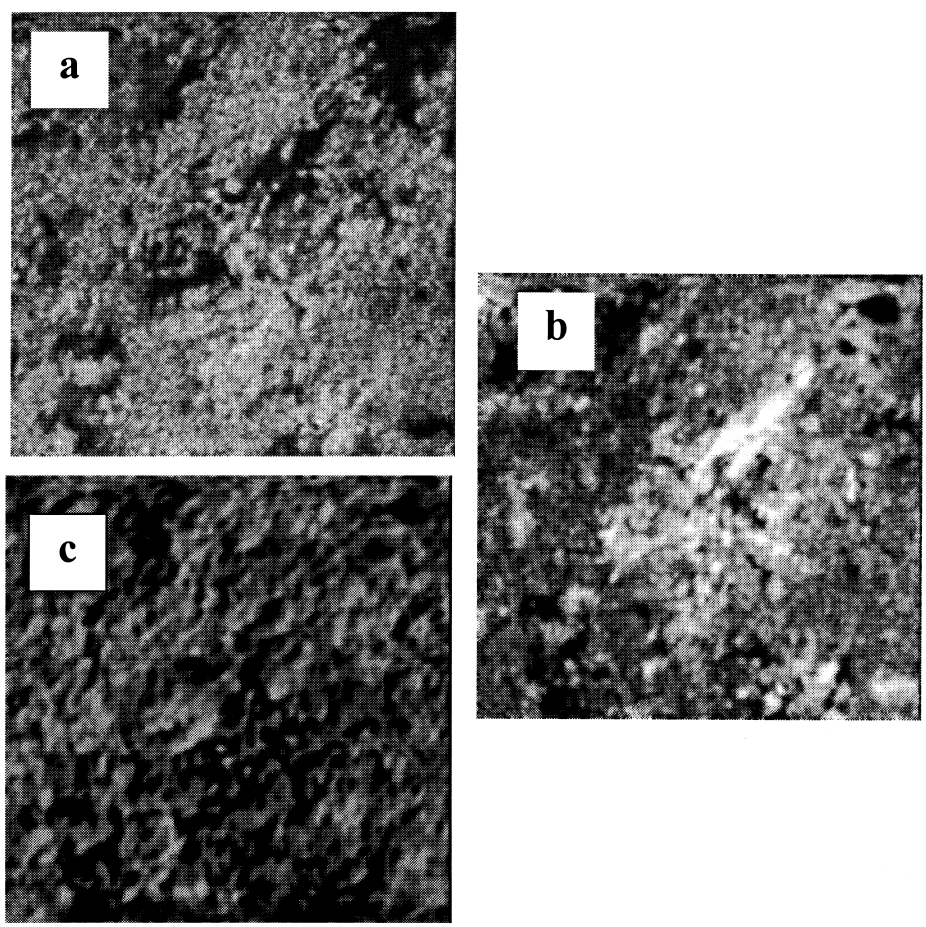

Fig. 7. Electron Probe Microscopic Analysis of cycled $LaNi_{4.27}Sn_{0.24}$ alloy electrode. The recorded X-ray intensities are compared with standard intensities of Ni (a), La (b) and O_2 (c). Lanthanum and oxygen rich phases suggest of alloy oxidation.

ies. Cycling was stopped when the storage capacity of hydrogen dropped to 70% of the maximum. Fig. 6 shows the cycling performance of bare, cobalt coated, and 25% cobalt mixed $LaNi_{4.27}Sn_{0.24}$ alloys. Bare alloy does not perform well under 0.3 C rate cycling conditions. It loses 70% of its capacity in less than 30 cycles. Cobalt coated alloys based on the thickness of deposited film, cycle better. It is seen that a very thin coating practically does not protect the alloy from corrosion. A 0.789 μm thick film of cobalt covers and protects the alloy for more than 180 cycles with constant capacity. Comparing this with the utilization studies in the previous section, it can be seen that the cobalt coating thickness can be optimized based on the cycle life requirements.

Alloy oxidation is believed to be one of the most important reasons for capacity decay. Oxidation of lanthanum to lanthanum oxides has been found to be an important cause of capacity decay. Studies have shown the diffusion of fresh lanthanum to the surface from the bulk, where it gets oxidized. Lanthanum oxidation results in the decrease of the dehydriding capacity of the electrode. Cobalt encapsulation forms as a protective cover over the alloy surface and prevents it from oxidation. The absence of protective cover in cobalt mixed electrodes is reflected in the capacity decay in those alloys. The surface coating also modifies the kinetics thereby improving the rate capability of the electrode.

3.5. Electron probe microscopic analysis (EPMA)

Recording the intensity of the characteristic X-ray line of an element while a beam is moved across the specimen can reveal the spatial distribution of that element. These intensities are compared to the standard intensities of the given species, namely lanthanum, nickel tin, cobalt, etc. by way of color maps. The color maps uses a scale that corresponds to a black body radiation, with concentration equated to the temperature. Thus the concentration of a particular species is high if the intensity map for that species is characterized by lot of white (bright) regions [18].

These recorded intensities on layered specimens however, depend on the layer thickness. The peak intensity is first converted to concentration and then using a hypothetical density (calculated based on molecular weights of composing elements), layer thickness is found.

X-ray map was obtained for a cycled metal hydride negative electrode made of bare $LaNi_{4.27}Sn_{0.24}$ alloy. Color maps comparing the recorded intensity with standard intensities of nickel (Fig. 7a), lanthanum (Fig. 7b) and oxygen (Fig. 7c) show that lanthanum and oxygen concentrations are very high in the alloy. This is due to the presence of lanthanum oxides that has formed during cycling.

On the other hand, lanthanum oxides are considerably absent in case of cobalt encapsulated alloys. Fig. 8 shows

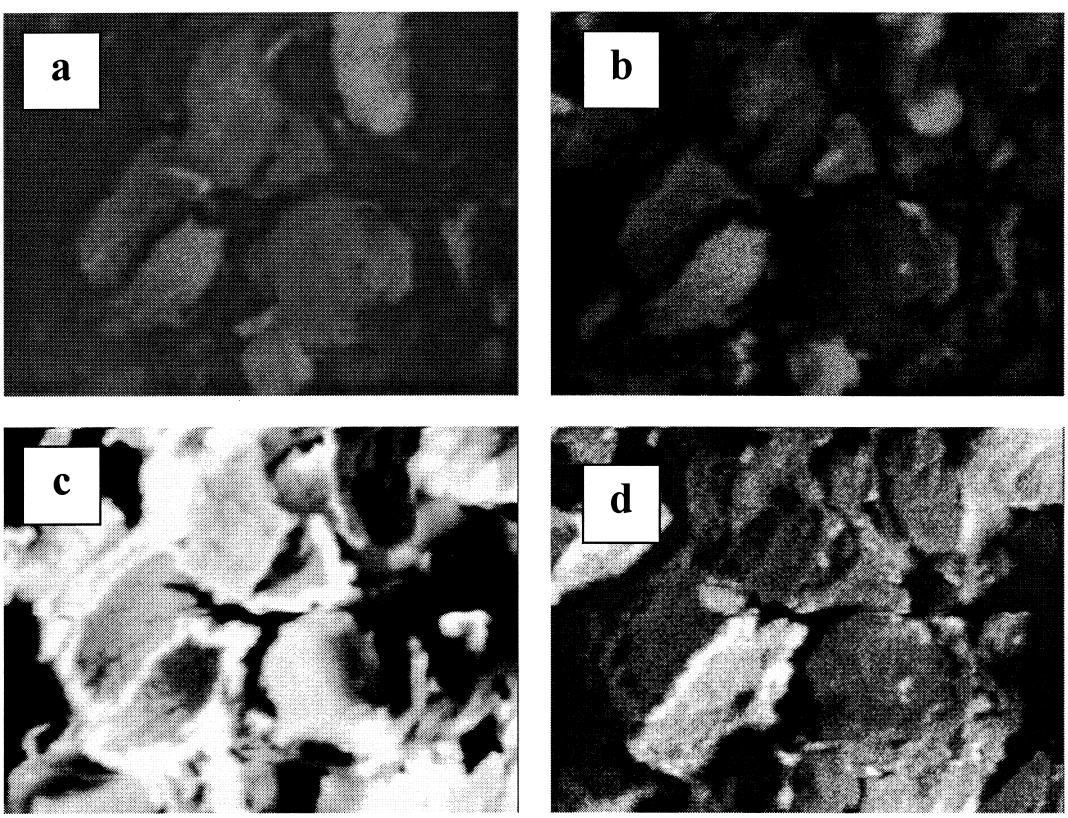

Fig. 8. EPMA of cycled cobalt coated $LaNi_{4.27}Sn_{0.24}$ alloy. The recorded X-ray intensities are compared with standard intensities of Ni (a), La (b) Co (c) and O_2 (d). Cobalt hydroxide present on the alloy surface protects the alloy from corrosion.

the X-ray map of cycled electrode made of cobalt encapsulated $LaNi_{4.27}Sn_{0.24}$ alloy compared for standard intensities of nickel (a), lanthanum (b), cobalt (c) and oxygen (d). Cobalt and oxygen rich phases confirm the presence of cobalt oxides on the alloy. It is seen that cobalt oxides that are present on the surface of the alloy protect it from oxidation.

4. Conclusions

$LaNi_{4.27}Sn_{0.24}$ alloy was treated using a surface modification technique wherein a thin film of cobalt was formed over the metal hydride alloy. Cobalt encapsulated electrodes have higher capacity and superior cycle life than bare alloy. Discharge curves show a second potential plateau at the end of the hydrogen desorption reaction. This is due to the cobalt faradaic reaction. Discharge studies done on pure cobalt show that this faradaic reaction clearly coincides with the second plateau during discharge of cobalt coated alloy. Cyclic voltammograms of the activated electrode reveal diffusion-limited hydrogen desorption as well as cobalt oxidation peaks during anodic potential sweep. The reverse scan shows the reduction of $Co(OH)_2$ to cobalt followed by the hydrogen absorption reaction. The utilization of pure cobalt was found to be very small as compared to that in the encapsulated case. Studies done using cobalt encapsulation of different thickness show that cobalt utilization increases with decrease in thickness. This is understandable from the fact that larger surface areas lead to better utilization of the active material. However, thinner coatings do not protect the metal hydride alloy from corrosion. Similarly, mixing $LaNi_{4.27}Sn_{0.24}$ with cobalt does not prevent the capacity fade. Optimization of film thickness was done and it is found that cobalt coating of 0.8 μm thick on the surface of the $LaNi_{4.27}Sn_{0.24}$ alloy gives a good protection for the alloy. The electrode cycled with a constant capacity for more than 200 cycles while the bare alloy failed within 30 cycles. The cycling studies were done at 0.3 C rate and this shows the high rate cyclability of cobalt coated electrodes. Further the EPMA diagrams for cycled bare alloy shows the presence of large amounts of oxidized (dead) alloy. Cobalt coated alloys have a protective layer of $Co(OH)_2$ over them and show no alloy oxidation. It is clearly seen that the cobalt coating protects the alloy from corrosion.

Acknowledgements

Financial support by the Exploratory Technology Research (ETR) program, which is supported by the Office of Transportation Technologies (OTT) of the U.S. Department of Energy (DOE), subcontract no. 4614610, is gratefully acknowledged.

References

[1] E.W. Justi, H.H. Eve, A.W. Kalberlah, N.M. Saridakis, M.H. Shaefer, Energy Convers. 10 (1970) 183.
[2] C. Iwakura, M. Matsuoka, Prog. Batts Batt. Mats 10 (1991) 81.
[3] J.J.G. Willems, Philips J. Res. 39 (1984) Suppl. 1.
[4] F. Meli, A. Zuttel, L. Schlapbach, J. Alloys Compounds 17 (1992) 190.
[5] B. Luan, N. Lui, H.J. Zhao, H.K. Liu, S.X. Dou, Int. J. Hydrogen Energy 21 (1996) 373.
[6] A. Durairajan, B.S. Haran, B.N. Popov, R.E. White, Studies on Hydrogen Diffusion in Metal Hydrides Using Impedance Spectroscopy, 194th Meeting of the Electrochemical Society, Boston, MA, Nov. 1998.
[7] B.S. Haran, B.N. Popov, R.E. White, J. Electrochem. Soc. 145 (1998) 3000.
[8] T. Weizhong, G. Yingxin, Z. Haoyu, J. Appl. Electrochem. 25 (1995) 874.
[9] D. Chartouni, F. Meli, A. Zuettel, K. Gross, L. Sclapbach, J. Alloys Compounds 241 (1996) 160.
[10] G. Zheng, B.N. Popov, R.E. White, J. Electrochem. Soc. 142 (1995) 2695.
[11] T. Sakai, A. Yuasa, H. Ishikawa, H. Miyamura, N. Kuriyama, J. Electrochem. Soc. 172 (1991) 1194.
[12] G. Zheng, B.N. Popov, R.E. White, J. Electrochem. Soc. 143 (1996) 834.
[13] B.N. Popov, Z. Koneska, J. Ivshin, D.M. Drazic, J. Serb. Chem. Soc. 54 (1989) 435.
[14] B.N. Popov, Z. Koneska, J. Ivshin, D.M. Drazic, J. Serb. Chem. Soc. 54 (1989) 443.
[15] R.P. Simpraga, J. Electroanal. Chem. 355 (1993) 79.
[16] M. Pourbaix, Atlas of Electrochemical Equilibria in Aqueous Solutions, Pergamon, Oxford, 1996, 322.
[17] H. Ishikawa, K. Ogura, A. Kato, H. Suzuki, J. Less-Common Metals 107 (1985) 105.
[18] S.J.B. Reed, Electron Microprobe Analysis and Scanning Electron Microscopy in Geology, Cambridge Univ. Press, Cambridge, 1993, 96.